eNeuro

Research Article: New Research | Development

Crucial Role of Rapgef2 and Rapgef6, a Family of Guanine Nucleotide Exchange Factors for Rap1 Small GTPase, in Formation of Apical Surface Adherens Junctions and Neural Progenitor Development in the Mouse Cerebral Cortex

Role of Rapgef2 and Rapgef6 in Neural Progenitors

Kazuhiro Maeta, Hironori Edamatsu, Kaori Nishihara, Junji Ikutomo, Shymaa E. Bilasy and Tohru Kataoka

Division of Molecular Biology, Department of Biochemistry and Molecular and Biology, Kobe University Graduate School of Medicine, 7-5-1 Kusunoki-cho, Chuo-ku, Kobe 650-0017, Japan

DOI: 10.1523/ENEURO.0142-16.2016

Received: 1 June 2016

Accepted: 4 June 2016

Published: 13 June 2016

Author Contributions: T. K. and K. M. designed research; K. M., J. I., K. N. and S. E. B. performed experiments; K.M., K.N., J.I., and S.E.B. contributed unpublished reagents/analytic tools; K. M., H. E., K. N., J. I. and T. K. analyzed data; T. K., H. E. and K. M. wrote the paper.

Funding: JSPS KAKENHI
20390080

Conflict of Interest: Authors report no conflict of interest.

Correspondence should be addressed to Tohru Kataoka, Division of Molecular Biology, Department of Biochemistry and Molecular Biology, Kobe University Graduate School of Medicine, 7-5-1 Kusunoki-cho, Chuo-ku, Kobe, 650-0017, Japan, E-mail: kataoka@people.kobe-u.ac.jp

Cite as: eNeuro 2016; 10.1523/ENEURO.0142-16.2016

1. Manuscript Title: Crucial Role of Rapgef2 and Rapgef6, a Family of Guanine Nucleotide Exchange Factors for Rap1 Small GTPase, in Formation of Apical Surface Adherens Junctions and Neural Progenitor Development in the Mouse Cerebral Cortex

2. Abbreviated Title: Role of Rapgef2 and Rapgef6 in Neural Progenitors

3. List all Author Names and Affiliations

Authors: Kazuhiro Maeta, Hironori Edamatsu, Kaori Nishihara, Junji Ikutomo, Shymaa E. Bilasy and Tohru Kataoka

Affiliations: Division of Molecular Biology, Department of Biochemistry and Molecular and Biology, Kobe University Graduate School of Medicine, 7-5-1 Kusunoki-cho, Chuo-ku, Kobe 650-0017, Japan

4. Author Contributions: T. K. and K. M. designed research; K. M., J. I., K. N. and S. B. performed experiments; K. M., H. E., K. N., J. I. and T. K. analyzed data; T. K., H. E. and K. M. wrote the paper.

5. Correspondence should be addressed to Tohru Kataoka, Division of Molecular Biology, Department of Biochemistry and Molecular Biology, Kobe University Graduate School of Medicine, 7-5-1 Kusunoki-cho, Chuo-ku, Kobe, 650-0017, Japan. E-mail: kataoka@people.kobe-u.ac.jp

6. Number of Figures: 7
7. Number of Tables: 0
8. Number of Multimedia: 0

9. Number of words for Abstract: 248
10. Number of words for Significance Statement: 119
11. Number of words for Introduction: 643
12. Number of words for Discussion: 1636

13. Acknowledgements: We thank Drs. Noboru Suzuki (Mie University), Koh-ichi Nagata (Aichi Human Service Center) and Fumio Matsuzaki (RIKEN Center for Developmental Biology) for generous donation of experimental materials. We also thank Dr. Toshio Terashima and Mr. Yoshiaki Sakihama (Kobe University Graduate

School of Medicine), Drs. Atsunori Shitamikai and Fumio Matsuzaki (RIKEN Center for Developmental Biology) and all of the members of our laboratory, especially Drs. Yoko Yoshikawa and Tatsuya Nagano, for valuable discussion.

Shymaa E. Bilasy's present address: Department of Biochemistry, Faculty of Pharmacy, Suez Canal University, El-shikh Zayed, Ismailia 41522, Egypt

14. Conflict of Interest: The authors declare no competing financial interests.

15. Funding sources: This work was supported by JSPS KAKENHI (Grant 20390080).

Key words: Rapgef2, Rapgef6, Rap1 small GTPase, neural progenitors, neocortex development, adherens junction

Abstract

Cerebral neocortex development in mammals requires highly orchestrated events involving proliferation, differentiation and migration of neural progenitors and neurons. Rapgef2 and Rapgef6 constitute a unique family of guanine nucleotide exchange factors for Rap1 small GTPase, which is known to play crucial roles in migration of post-mitotic neurons. We previously reported that conditional knockout of *Rapgef2* in dorsal telencephalon (*Rapgef2*-cKO) resulted in formation of an ectopic cortical mass (ECM) resembling that of subcortical band heterotopia. Here we show that additional knockout of *Rapgef6* in *Rapgef2*-cKO mice (*Rapgef2/6*-dKO) results in marked enlargement of the ECM. While *Rapgef2*-cKO affects late-born neurons only, *Rapgef2/6*-dKO affects both early-born and late-born neurons. The *Rapgef2*-cKO cortex at embryonic day (E) 15.5 and the *Rapgef2/6*-dKO cortex at E13.5 and E15.5 show disruption of the adherens junctions (AJs) on the apical surface, detachment of radial glial cells (RGCs) from the apical surface and disorganization of the radial glial fiber system, which are accompanied by aberrant distribution of RGCs and intermediate progenitors, normally located in the ventricular zone (VZ) and the subventricular zone, respectively, over the entire cerebral cortex. Moreover, intrauterine transduction of Cre recombinase into the *Rapgef2*$^{flox/flox}$ brains also results in the apical surface AJ

disruption and the RGC detachment from the apical surface, both of which are effectively suppressed by co-transduction of the constitutively active Rap1 mutant, $Rap1^{G12V}$. These results demonstrate a cell-autonomous role of the Rapgef2/6-Rap1 pathway in maintaining the apical surface AJ structures, which is necessary for the proper development of neural progenitor cells.

Significance Statement

Rapgef2 is known to play a critical role in multipolar-bipolar transition of post-mitotic neurons from shRNA-mediated knockdown experiments. This function of Rapgef2 was presumed to account for the formation of an ectopic cortical mass observed in *Rapgef2* conditional knockout (*Rapgef2*-cKO) mice. In this manuscript, by utilizing *Rapgef2*-cKO mice and the intrauterine electroporation method, we are able to demonstrate a novel role of the Rapgef2-Rap1 pathway in proper development of neural progenitors, particularly RGCs, which is presumably accounted for by its cell-autonomous role in maintaining the apical surface AJ structures. Moreover, we show that Rapgef6, a close Rapgef2 homologue implicated in the etiology of schizophrenia, shares some of these functions with Rapgef2 from the examination of *Rapgef2/6* double knockout mice.

Introduction

One of the hallmarks of the mammalian cerebral neocortex is that neurons with distinct morphology and functions are organized into 6 horizontal layers (Defelipe, 2011). In mice, layer formation occurs between embryonic day 11 (E11) and E18 in an inside-out manner, where waves of post-mitotic neurons migrate successively through the previously formed layers (Hoerder-Suabedissen and Molnár, 2015). During neurogenesis, radial glial cells (RGCs), located in the ventricular zone (VZ), function as neural progenitors and generate self-renewing RGCs and neurons as well as committed intermediate progenitor cells (IPCs). IPCs move to the subventricular zone (SVZ), divide and differentiate into neurons. Newly-born neurons adopt multipolar morphology and migrate to the intermediate zone (IZ), where they undergo multipolar-bipolar transition to assume bipolar morphology and migrate along the radial glial (RG) fibers to the cortical plate, a process called RG fiber-guided locomotion. Finally, they undergo RG fiber-independent somal translocation to reach their final destinations, a process called terminal translocation. Concurrently, the somata of RGCs undergo radial translocation throughout the width of the VZ depending on the phases of the cell cycle; the somata of S phase and M phase cells are located at the basal and apical sides, respectively. This confers the VZ a false stratified appearance. Each RGC possesses two

RG fibers: a basal fiber, which reaches the pial surface and serves as a scaffold for neuronal migration, and an apical fiber, whose endfoot establishes adherens junctions (AJs) with those of neighboring RGCs and forms the apical surface of the telencephalon lining the ventricles.

Rap1, consisting of two isoforms Rap1a and Rap1b, is a close homologue of Ras small GTPases and plays pleiotropic functions controlling cell proliferation, adhesion, polarity and endocytosis (Gloerich and Bos, 2011). In particular, it plays a pivotal role in regulation of the integrin-mediated and the cadherin-mediated cell adhesion (Boettner and Van Aelst, 2009). Like other GTPases, Rap1 functions as a molecular switch by cycling between GTP-bound active and GDP-bound inactive forms. Their interconversion is reciprocally stimulated by guanine nucleotide exchange factors (GEFs) and GTPase-activating proteins (GAPs), where GEFs mediate Rap1 activation in response to various extracellular stimuli. There exist an array of GEFs for Rap1 including Rapgef1 to 6, RasGEF1A to C, CalDAG-GEF1/3 and phospholipase Cε, which are regulated by distinct signaling mechanisms and responsible for differential regulation of Rap1 activity in spatial, temporal and cell-type-specific manners (Gloerich and Bos, 2011). During the mouse cerebral neocortex development, Rap1 was shown to play crucial roles in neuronal migration, particularly in the multipolar migration, the

multipolar-bipolar transition and the terminal translocation but not the RG fiber-guided locomotion (Voss *et al.,* 2008; Franco *et al.*, 2011; Jossin and Cooper, 2011; Sekine *et al.,* 2012). In these cases, Rapgef1, also called C3G, was shown to be involved in Rap1 activation downstream of the Reelin-Reelin receptors-Dab1-Crk/CrkL signaling.

Rapgef2, also called RA-GEF-1 and PDZ-GEF1 (de Rooij *et al.,* 1999; Liao *et al.*, 1999, 2001), and Rapgef6, also called RA-GEF-2 (Gao *et al.*, 2001), constitute a unique Rap1-GEF family characterized by the possession of the PSD-95/DlgA/ZO-1 and Ras/Rap-associating domains. Through association with the GTP-bound forms of Rap1 and M-Ras at the Ras/Rap-associating domains, they are recruited from the cytoplasm to the Golgi complex and the plasma membranes, respectively, and cause Rap1 activation by the action of their CDC25-homology domains. We showed that dorsal telencephalon-specific *Rapgef2* conditional knockout (*Rapgef2*-cKO) mice develop an ectopic cortical mass (ECM) resembling that of subcortical band heterotopia, suggesting a role of Rapgef2 in neocortical development (Bilasy *et al.*, 2009). Recently, Rapgef2 was reported to play a crucial role in the multipolar-bipolar transition of post-mitotic neurons (Ye *et al.,* 2014).

In this study, we observe severe defects in the development of RGCs and IPCs and the formation of the apical surface AJs in the developing cerebral cortices of

Rapgef2-cKO and *Rapgef2/Rapgef6*-double knockout (*Rapgef2/6*-dKO) mice, revealing a novel role of the Rapgef2/6-Rap1 pathway in neural progenitor cells.

Materials and Methods

Animals. *Rapgef2*$^{flox/flox}$ (*Rapgef2*-f/f) and *Rapgef6*$^{-/-}$ mice were generated as reported before (Bilasy *et al.*, 2009; Yoshikawa *et al.*, 2007). *Rapgef2*-cKO mice were generated by mating *Rapgef2*-f/f mice with *Emx1*$^{cre/+}$ mice as described (Bilasy *et al.*, 2009). *Rapgef6*-KO mice used in this study were *Rapgef2*$^{flox/flox}$;*Rapgef6*$^{-/-}$ mice. *Rapgef2/6*-dKO mice were generated by mating them with *Emx1*$^{cre/+}$ mice. Genotypes were determined by polymerase chain reaction (PCR) as described before (Bilasy *et al.*, 2009; Yoshikawa *et al.*, 2007). All the animals had been backcrossed to C57BL/6JJcl mice (http://jaxmice.jax.org/strain/013636.html) over 8 times and maintained on 12-h light/dark cycles with free access to food and water. To obtain embryos, female mice were placed together with a male mouse overnight and the following morning (~10:00 a. m.) was defined as E0.5. Operations were carried out under general anesthesia by an intraperitoneal administration of dexmedetomidine (0.3 mg/kg; Maruishi Pharmaceutical, Osaka, Japan), midazolam (4 mg/kg; Astellas Pharma, Osaka, Japan) and butorphanol tartrate (5 mg/kg; Meiji Seika Pharma, Tokyo, Japan) as described

(Nagano *et al.,* 2014). The use and care of the animals were reviewed and approved by the Institutional Animal Care and Use Committee of Kobe University.

Antibodies. Following primary antibodies were used for indirect immunofluorescence staining: anti-Cux1 (sc-13024; Santa Cruz Biotechnology), anti-Ctip2 (ab18465; Abcam), anti-green fluorescent protein (GFP) (GFP-1010; Aves Labs), anti-Pax6 (PD022; MBL), anti-bromodeoxyuridine (BrdU) (555627; BD Biosciences), anti-phospho-histone-H3(Ser10) (09-797; Millipore), anti-Rapgef2 (Wei *et al.,* 2007), anti-Rapgef6 (Yoshikawa *et al.,* 2007), anti-β-catenin (610153; BD Biosciences), anti-N-cadherin (610920; BD Biosciences), anti-E-cadherin (610181; BD Biosciences), anti-afadin (ab90809; Abcam), anti-zonula occludens-1 (ZO-1) (61-7300; Life Technologies), anti-nestin (556309; BD Biosciences), anti-Tbr1 (ab31940; Abcam), and anti-c-Myc (23941-54; Nacalai Tesque), antibodies. To detect immunoreactive signals, following secondary antibodies were used: Alexa Fluor 488-conjugated anti-chicken immunoglobulin (Ig) Y (703-545-155; Jackson Immuno Research), Alexa Fluor 647-conjugated anti-rabbit IgG (A21244; Life Technologies), CF647-conjugated anti-mouse IgG (20281; Biotium), CF488A-conjugated anti-IgG (20302, 20015, 20027; Biotium), CF488A anti-mouse IgG (Biotium) and CF555-conjugated anti-IgG (20231,

20038, 20233; Biotium) antibodies. An Alexa Fluor 647-conjugated anti-Tbr2 antibody (51-4875; eBioscience) was also used.

Plasmids. A Cre recombinase-expression vector, pCAG-NLS-Cre (Tsumura *et al.*, 2006), was provided by Dr. N. Suzuki (Mie University, Tsu, Japan). pCAG=EGFP, an expression vector of enhanced GFP (EGFP) (Nishimura et al., 2014), was a gift from Dr. K. Nagata (Aichi Human Service Center, Kasugai, Japan). pCAG-FloxP-EGFP-N1, which conditionally expresses EGFP in cells harboring Cre recombinase (Shitamukai *et al*., 2011), and pCAG-EGFP-F, which expresses EGFP attached with a C-terminal CAAX motif, the farnesylation signal, were provided by Dr. F. Matsuzaki (RIKEN Center for Developmental Biology, Kobe, Japan). pCAG-Myc-Rap1^{WT} and pCAG-Myc-Rap1^{G12V}, which express wild-type Rap1 and Rap1^{G12V} attached with an N-terminal human c-Myc epitope tag, respectively, were generated by cloning the respective cDNAs (Liao *et al*., 1999) into a *Bam*HI cleavage site of a derivative of pCAG=MCS2 (Kawauchi *et al*., 2005).

Immunofluorescence. Preparation of histologic samples and immunostaining were performed as described previously (Bilasy *et al.,* 2009). Serial sections (6-µm thick) of paraffin-embedded specimens and serial sections (20-µm or 50-µm thick) of frozen specimens were cut on a sliding microtome (SM2000R; Leica) and a cryostat (CM1850;

Leica), respectively. Immunofluorescently-stained sections were observed under a confocal laser scanning microscope (LSM510 META; Carl Zeiss), and, if necessary, the focus stacking technique (also known as *z*-stacking) was employed to digitally combine multiple images taken at different focus distances of each section. Hematoxylin and eosin (H&E)-stained sections were observed under an AX80 microscope with a DP70 camera (Olympus).

Assessment of cell distribution. Radial distributions of neural progenitors and neurons were quantified essentially as described (Franco *et al.*, 2011). Briefly, the neocortex and ECM were separately divided into 10 laminar bins with equal thickness and width, and cells in each bin were counted. The percentage of the cells present in each bin was obtained as follows: 100 × the number of cells in each bin/the total number of cells in the 10 bins.

BrdU labeling. BrdU was dissolved in sterile saline and intraperitoneally injected into pregnant females at a dose of 100 μg/g bodyweight. To detect S phase cells, brain specimens of their embryos were harvested 0.5 h later, fixed in 4% paraformaldehyde and subjected to immunohistological detection of BrdU. To trace the progenitor fate, embryonic brains were harvested at various time points and analyzed as described above.

In utero electroporation (IUE). IUE was performed at E14.5 using an electroporator (CUY21 EDIT II; BEX Co, Ltd.) along with a pair of forceps-type electrodes as described (Saito and Nakatsuji, 2001). The lateral ventricle of an embryo received 1 µl of sterilized water containing 0.01% FastGreen dye and the following plasmids: pCAG-EGFP-F (0.01 µg/µl) for labeling cells with farnesylated EGFP, pCAG-NLS-Cre (0.1 µg/µl) and pCAG-FloxP-EGFP-N1 (0.5 µg/µl) for deleting *Rapgef2* in *Rapgef2*-f/f embryos, pCAG=EGFP (0.5 µg/µl) for labeling cells without *Rapgef2* deletion in *Rapgef2*-f/f embryos, and pCAG-NLS-Cre (0.05 µg/µl), pCAG-FloxP-EGFP-N1 (0.25 µg/µl) and either pCAG-Myc-Rap1^{WT}, pCAG-Myc-Rap1^{G12V} or pCAG-Myc (0.7 µg/µl each) for testing the compensation by Rap1. Subsequently, electroporation was performed by 450-ms pulses of 30 V separated by 980 ms.

Reproducibility and Statistical analysis. Images shown are representatives of ones obtained from at least 3 biological replicates. For graphs, data are expressed as the means ± SDs derived from biologically independent replicates whose numbers are indicated in their figure legends. If *p* value obtained by the unpaired two-tailed Student's *t*-test was smaller than 0.05, the difference was considered statistically significant.

Results

Effects of *Rapgef2*-cKO and *Rapgef2/6*-dKO on the cortical architecture

Rapgef2-cKO mice had been shown to develop severe brain malformations characterized by formation of a large ECM lacking the layer structure beneath a thin neocortex retaining the typical 6-layered structure, interruption of the pyramidal cells in the hippocampal CA1 region, enlargement of the lateral ventricles and agenesis of interhemispheric connections (Bilasy *et al.,* 2009, 2011). The ECM extended throughout the rostro-caudal axis of the cerebral hemisphere. On the other hand, the brains of *Rapgef6*-KO mice failed to show any morphological abnormalities (Yoshikawa *et al.,* 2007; Levy *et al.,* 2015).

Considering the structural and functional similarity between Rapgef2 and Rapgef6, we first examined the effects of *Rapgef6* knockout on the brain malformations of *Rapgef2*-cKO mice by generating *Rapgef2/6*-dKO mice. At postnatal day (P) 90, *Rapgef2/6*-dKO mice showed more severe brain malformations compared to *Rapgef2*-cKO mice, characterized by an enlarged ECM beneath a very thin neocortex and generalized atrophy of the hippocampus (Fig. 1*A*). Also, agenesis of the corpus callosum was evident. As reported before, the *Rapgef6*-KO brains did not show any

morphological abnormalities as compared to those of *Rapgef2*-f/f mice, which were used as a control throughout this study. Cortical layer structures were examined by immunostaining for Ctip2 and Cux1 to visualize early-born neurons in the layers V/VI, born between E12.5 and E13.5, and late-born neurons in the layers II/III and IV, born between E14.5 and E18.5, respectively (Fig. 1*B,C*) (Greig *et al.*, 2013). The thin neocortices of *Rapgef2*-cKO and *Rapgef2/6*-dKO mice kept an inside-out laminar organization as observed in the neocortices of *Rapgef2*-f/f and *Rapgef6*-KO mice. In contrast, their ECMs lost the laminar organization altogether. Neurons residing in the *Rapgef2*-cKO ECM were mostly composed of $Cux1^+$ neurons while those in the *Rapgef2/6*-dKO ECM were composed of a mixture of nearly equal numbers of $Ctip2^+$ and $Cux1^+$ neurons (Fig. 1*B,D*). Consistent with this, the *Rapgef2/6*-dKO neocortices showed a significant reduction in the numbers of both $Ctip2^+$ and $Cux1^+$ neurons while the *Rapgef2*-cKO neocortices showed a reduction in the number of $Cux1^+$ neurons only (Fig. 1*D*). These observations indicated that both early-born and late-born neurons were almost evenly affected by *Rapgef2/6*-dKO whereas late-born neurons were predominantly affected by *Rapgef2*-cKO. The present results obtained with *Rapgef2*-cKO mice were indistinguishable from those with *Rapgef2*-cKO mice on the mixed background of ICR and C57BL/6J (Bilasy *et al.*, 2009).

On the other hand, the total numbers of Ctip2$^+$ neurons and Cux1$^+$ neurons showed a substantial increase in the *Rapgef2/6*-dKO cortices while that of Cux1$^+$ neurons only showed an increase in the *Rapgef2*-cKO cortices (Fig. 1*D*), hinting that an expansion of the neural progenitor pools for the affected neurons might have occurred in *Rapgef2*-cKO and *Rapgef2/6*-dKO embryos.

Effects of *Rapgef2*-cKO and *Rapgef2/6*-dKO on distribution of neural progenitors in the developing cerebral cortex

To gain an insight into the mechanism for the ECM formation, we next examined the courses of brain development of *Rapgef2*-cKO and *Rapgef2/6*-dKO embryos at E13.5 and E15.5, when early-born neurons and late-born neurons, respectively, were predominantly generated (Greig *et al.*, 2013). Differentiation from RGCs to neurons could be traced by sequential alterations in the expression of the transcription factors: Pax6 in RGCs and Tbr2 in IPCs (Englund *et al.*, 2005). At E13.5 and E15.5, Pax6$^+$ RGCs and Tbr2$^+$ IPCs were exclusively located in the VZ (bins 1-5 at E13.5 and bins 1-3 at E15.5) and the SVZ (bins 6-8 at E13.5 and bins 2-4 at E15.5), respectively, in the *Rapgef2*-f/f and *Rapgef6*-KO cortices (Fig. 2*A*,*B*). On the other hand, at E13.5 in the *Rapgef2*-cKO cortices, minor but significant populations of Pax6$^+$ cells and Tbr2$^+$ cells were also located at the basal side (bins 9 and 10). Strikingly, in the *Rapgef2*/6-dKO

cortices, both Pax6$^+$ cells and Tbr2$^+$ cells were scattered almost evenly over their entire thickness at both E13.5 and E15.5. Moreover, at E15.5, the cortex-wide scattering of both Pax6$^+$ RGCs and Tbr2$^+$ IPCs became also evident in the *Rapgef2*-cKO cortices (Fig. 2*A,B*). Similar to the observation with neurons at P90, the total numbers of Pax6$^+$ RGCs and Tbr2$^+$ IPCs were substantially increased at both E13.5 and E15.5 in the *Rapgef2/6*-dKO cortices and at E15.5 only in the *Rapgef2*-cKO cortices (Fig. 2*C*). Consistent with this, a substantial increase in the cortical thickness was observed in *Rapgef2/6*-dKO brains at both E13.5 and E15.5 and in the *Rapgef2*-cKO brains at E15.5 only (Fig. 2*A*).

Next, we used BrdU labeling to visualize cells in S phase of the cell cycle (Fig. 2*A*). At E13.5, almost all BrdU$^+$ cells were also positive for either Pax6 or Tbr2 and located at the basal side of the VZ and the apical side of the SVZ, respectively, in the *Rapgef2*-f/f and *Rapgef6*-KO cortices. On the other hand, in the *Rapgef2*-cKO cortices at E13.5, minor but significant populations of BrdU$^+$/Pax6$^+$ cells and BrdU$^+$/Tbr2$^+$ cells were located ectopically at the basal side (bins 9 and 10). At E15.5, both BrdU$^+$/Pax6$^+$ cells and BrdU$^+$/Tbr2$^+$ cells were evenly scattered over the entire cortices. Notably, the *Rapgef2/6*-dKO cortices showed similar cortex-wide scattering of both BrdU$^+$/Pax6$^+$ cells and BrdU$^+$/Tbr2$^+$ cells by E13.5. Furthermore, the *Rapgef2*-cKO and

Rapgef2/6-dKO cortices showed an essentially similar pattern of the ectopic localization of metaphase cells, which were visualized by immunostaining for phospho-histone-H3(Ser10) (pHH3) (Fig. 2*D*). Notably, in the *Rapgef2/6*-dKO cortices at both E13.5 and E15.5 and the *Rapgef2*-cKO cortices at E15.5 only, $pHH3^+/Pax6^+$ and $pHH3^+/Tbr2^+$ cells lost their normal localizations at the apical sides of the VZ and the SVZ, respectively, and were almost evenly scattered over their entire thickness. The percentages of $pHH3^+/Pax6^+$ cells located in close proximity to the apical surface were markedly reduced in the *Rapgef2/6*-dKO cortices at both E13.5 and E15.5 and the *Rapgef2*-cKO embryos at E15.5 only, compared to almost 100% in the *Rapgef2*-f/f and *Rapgef6*-KO cortices at both E13.5 and 15.5 (Fig. 2*E*). As observed with $Pax6^+$ and $Tbr2^+$ cells, the total numbers of $pHH3^+/Pax6^+$ and $pHH3^+/Tbr2^+$ cells were substantially increased at both E13.5 and E15.5 in the *Rapgef2/6*-dKO cortices and at E15.5 only in the *Rapgef2*-cKO cortex (Fig. 2*F*). Similar ectopic localization of metaphase RGCs had been observed in mice deficient in AJ proteins (Kadowaki *et al*., 2006; Lien *et al*., 2006; Gil-Sanz *et al*., 2014; Yamamoto *et al*., 2015).

Effects of *Rapgef2*-cKO and *Rapgef2/6*-dKO on the apical surface structure in the developing cerebral cortex

We next analyzed the expression pattern of Rapgef2 and Rapgef6 in the developing cerebral cortex. Immunostaining of the E13.5 brain sections showed that both Rapgef2 and Rapgef6 were expressed throughout the cortices with a higher extent of expression at the apical surface (Fig. 3*A*). However, at E15.5 Rapgef6 disappeared from the VZ/SVZ and IZ and the apical part of the CP whereas Rapgef2 retained an expression pattern similar to that observed at E13.5. The specificities of the immunostaining were verified by disappearance of the immunoreactive signals concomitant with the knockout of the corresponding genes. The apical surface structure lining the ventricles is composed of an assembly of the endfeet of the apical RG fibers, which are linked together by an array of the AJs (Götz and Huttner, 2005). Both Rapgef2 and Rapgef6 at E13.5 and Rapgef2 only at E15.5 were concentrated at the AJs on the apical surface as shown by their colocalization with β-catenin (Fig. 3*B*). Considering that the constituents of the AJs, such as β-catenin, N-cadherin, E-cadherin, afadin and ZO-1, play critical roles in formation of the apical surface structure and that ablation of their individual functions led to ECM formation similar to that observed in the *Rapgef2*-cKO brain (Machon *et al.*, 2003; Junghans *et al.*, 2005; Lien *et al.*, 2006; Kadowaki *et al.*, 2007; Schmid *et al.*, 2014; Gil-Sanz *et al.*, 2014; Yamamoto *et al.*, 2015), we examined the apical surface morphology of the *Rapgef2*-cKO and *Rapgef2/6*-dKO cortices (Fig. 4).

Strikingly, in the *Rapgef2/6*-dKO cortices at both E13.5 and E15.5, their apical surfaces became very irregular and heavily disintegrated so that a significant population of cells were apparently exfoliated from the surfaces into the ventricle (Fig. 4*A,B*, *leftmost panels*). The *Rapgef2*-cKO cortices showed less severe morphological abnormalities; the apical surfaces looked almost intact at E13.5 but assumed irregular morphology at E15.5. The formation of the AJs lining the apical surface was further examined by immunostaining for β-catenin, N-cadherin, E-cadherin, afadin and ZO-1, all of which were concentrated there in the *Rapgef2*-f/f and *Rapgef6*-KO cortices at E13.5 and E15.5 (Fig. 4*A,B*). Strikingly, in the *Rapgef2/6*-dKO cortices, a dense array of the apical surface AJs became almost nonexistent at both E13.5 and E15.5. Again, the *Rapgef2*-cKO cortices showed less severe abnormalities; the disappearance of the AJs was not clearly recognizable until E15.5.

Effects of *Rapgef2*-cKO and *Rapgef2/6*-dKO on the RG fiber organization

Regarding the past studies showing that AJ disruption impaired the scaffolding of RGCs on the apical surface and caused a disturbance of the RG fiber organization (Kadowaki *et al.*, 2007; Yamamoto *et al.*, 2015), we examined RG fiber morphology in the *Rapgef2*-cKO and *Rapgef2/6*-dKO cortices by immunostaining for nestin. In the *Rapgef2*-f/f and *Rapgef6*-KO cortices, nestin^{+} RG fibers showed regular radial

355 alignment spanning their entire thickness and reaching the pial surface (Fig. 5*A*).
356 Notably, in the *Rapgef2*/*6*-dKO cortices at both E13.5 and E15.5, the RG fiber system
357 was heavily disorganized; RG fibers were randomly oriented throughout their entire
358 thickness. Moreover, the RG fibers seemed to be broken down into short pieces at E15.5,
359 which might reflect the dispersion of RGCs throughout the cortices. On the other hand,
360 in the *Rapgef2*-cKO cortices, the disorganization of RG fibers was not clearly
361 recognizable until E15.5 when RG fibers showed disoriented and irregular arrangements
362 more prominent in the lower zones including the SVZ/VZ and IZ than in the upper
363 zones including the CP. The time course of the RG fiber disorganization apparently
364 correlated with that of the apical surface AJ disruption. Next, IUE-mediated
365 transduction of pCAG-EGFP-F, expressing plasma membrane-localized EGFP, into
366 E14.5 *Rapgef2*-cKO embryos was employed to more clearly observe the RG fiber
367 morphology in the E15.5 cortices (Fig. 5*B*). While the basal fibers of the ectopically
368 located $Pax6^+$ RGCs looked almost intact reaching the pial surface, the apical fibers
369 became shorter or almost nonexistent and seemed to be disconnected from the apical
370 surface.

371 At the same time, we examined the migration of $Ctip2^+$ neurons, which is dependent
372 on the RG fiber-guided locomotion. In the *Rapgef2*-f/f and *Rapgef6*-KO cortices, $Ctip2^+$

neurons were almost exclusively located in the CP at E13.5 and E15.5 (Fig. 5*C*). In sharp contrast, in the *Rapgef2/6*-dKO cortices, most of Ctip2^{+} neuron failed to reach the CP and were located in the lower zones at E15.5. The sign of this migration delay was already evident at E13.5. In the *Rapgef2*-cKO cortices, the location of Ctip2^{+} neurons looked normal at E13.5. However, a small but significant proportion of Ctip2^{+} neurons were located in the lower zones at E15.5. These results suggested the existence of a certain correlation between the extents of RG fiber disorganization and the neuronal migration disorder. Also, the ectopic accumulation of neurons observed at E15.5 was likely to be a predecessor of the ECM formed in the adult *Rapgef2*-cKO and *Rapgef2*/*6*-dKO cortices.

Cell-autonomous function of Rapgef2 in neural progenitors and role of its Rap1-GEF activity

To examine the cell-autonomous function of Rapgef2, we introduced *Rapgef2* knockout into RGCs lining the apical surface by IUE-mediated transduction of pCAG-NLS-Cre, expressing Cre recombinase, into *Rapgef2*-f/f embryos at E14.5. Cells harboring the Cre-expression vector were marked by GFP through co-transduction of pCAG-FloxP-EGFP-N1, which conditionally expresses EGFP in cells expressing Cre recombinase (Shitamukai *et al*., 2011). Hereafter the resulting embryos are called

391 *Cre/cEGFP*. As control, RGCs were labeled with GFP by IUE-mediated transduction of
392 pCAG=EGFP into *Rapgef2*-f/f and *Rapgef2*-cKO embryos at E14.5 to trace their fate
393 and the resulting embryos are called *EGFP/Rapgef2*-f/f and *EGFP/Rapgef2*-cKO,
394 respectively. When examined at E16.5, Rapgef2 expression was successfully eliminated
395 in GFP^+ cells in the *Cre/cEGFP* cortices (Fig. 6*A*). In *EGFP/Rapgef2*-cKO embryos at
396 E16.5, $Pax6^+/GFP^+$ cells, exclusively located in the VZ in the case of *EGFP/Rapgef2*-f/f
397 embryos, almost completely disappeared from the VZ and were mainly located in the IZ
398 and CP as observed with $Pax6^+$ cells as a whole (Fig. 6*B*, also see Fig. 2*A*, *B*). Likewise,
399 the majority of $Tbr2^+/GFP^+$ cells, predominantly located in the SVZ in
400 *EGFP/Rapgef2*-f/f embryos, showed ectopic localization in the IZ and CP in
401 *EGFP/Rapgef2*-cKO embryos as observed with $Tbr2^+$ cells as a whole. Likewise, in
402 *Cre/cEGFP* embryos at E16.5, the proportion of $Pax6^+/GFP^+$ cells was also markedly
403 decreased in the VZ, which was accompanied by an increase in the proportion of GFP^+
404 cells located in the IZ (Fig. 6*B, C*). However, the GFP^+ cells in the IZ were totally
405 negative for Pax6 or Tbr2, indicating that they lost the progenitor property. The
406 distribution of $Tbr2^+/GFP^+$ cells appeared not significantly affected (Fig. 6*B, C*). The
407 apical surface of the *EGFP/Rapgef2*-cKO cortices showed very irregular cell
408 arrangements and disappearance of the apical fiber endfeet of $Pax6^+/GFP^+$ cells, which

was accompanied by the loss of the apical fibers in $Pax6^{+}/GFP^{+}$ cells (Fig. 6*D*). Moreover, immunostaining for Pax6 and afadin showed that the AJs on the apical surface became almost nonexistent. These results were consistent with the observation with the *Rapgef2*-cKO cortices at E15.5 and the *Rapgef2/6*-dKO cortices at E13.5 and E15.5 (Fig. 4). In the *Cre/cEGFP* cortices, the numbers of GFP^{+} apical fibers and their endfeet on the apical surface were also substantially reduced and the apical surface AJs were compromised as shown by immunostaining for afadin (Fig. 6*D*). These results taken together indicated that Rapgef2 possesses a cell-autonomous function in maintaining the apical surface AJ structures and preventing earlier detachment of RGCs from the apical surface. However, a non-cell-autonomous effect of the *Rapgef2* knockout seems to be responsible for preservation of the progenitor properties in RGCs and IPCs detached from the apical surface observed in the *Rapgef2*-cKO cortices.

To clarify whether the function of Rapgef2 in RGCs was governed by their GEF activity toward Rap1, we examined the effects of artificial expression of $Rap1^{G12V}$, the constitutively active Rap1 mutant which had its GTPase activity severely impaired and did not rely on Rap1-GEFs for its activation. $Rap1^{WT}$, wild-type Rap1, whose activity was dependent on Rap1-GEFs, was used as a control. To this end, either pCAG-Myc-$Rap1^{G12V}$, pCAG-Myc-$Rap1^{WT}$ or pCAG-Myc empty vector was

transduced by IUE into *Rapgef2*-f/f embryos in combination with both pCAG-NLS-Cre and pCAG-FloxP-EGFP-N1 at E14.5. When observed at E16.5, the co-transduction of pCAG-Myc-Rap1^{G12V} but not pCAG-Myc-Rap1^{WT} or pCAG-Myc successfully restored not only the proportion of Pax6^{+}/GFP^{+} cells in the VZ (Fig. 6*E*, *F*) but also the numbers of the apical fibers and their endofeet and the density of the apical surface AJs (Fig. 6*G*) to the extent comparable to that of the *EGFP/Rapgef2*-f/f cortex (Fig. 6*B*, *C*, *D*). These results indicated that the Rap1-GEF activity of Rapgef2 was responsible for its function in maintaining the apical surface AJ structures and preventing earlier detachment of RGCs from the apical surface.

Cell-autonomous and non-cell-autonomous functions of Rapgef2 on neuronal migration

Rap1 plays crucial roles in neuronal migration, particularly in the multipolar migration, the multipolar-bipolar transition and the terminal translocation (Voss *et al.*, 2008; Franco *et al.*, 2011; Jossin and Cooper, 2011; Sekine *et al.*, 2012; Ye *et al.*, 2014). To clarify the role of Rapgef2 in neuronal migration, the morphology and location of neurons labeled with GFP by IUE at E14.5 were examined at P7 in *EGFP/Rapgef2*-f/f and *EGFP/Rapgef2*-cKO mice (Fig. 7*A*). In the *EGFP/Rapgef2*-f/f cortices, GFP^{+} cells were late-born neurons positive for Cux1 and almost exclusively located in the layers

II-IV (Fig. 7*A*, *B*). In contrast, consistent with the ECM formation predominantly consisting of late-born neurons, almost all of GFP^+ cells, which were also positive for Cux1, were located in the ECM in the *EGFP/Rapgef2*-cKO cortices. Notably, about a half of them assumed multipolar morphology (Fig. 7*C*), suggesting that an impairment of the multipolar-bipolar transition caused the defect in neuronal migration. To examine the cell-autonomous effect of the *Rapgef2* knockout, we observed the morphology and location of neurons at P7 in *Cre/cEGFP* mice. Notably, almost all of $Cux1^+/GFP^+$ neurons successfully reached the layers II-IV (Fig. 7*A*, *B*). Closer inspection revealed that they were mainly located in the upper section probably corresponding to the layer II-III rather than the lower section probably corresponding to the layer IV observed in the *EGFP/Rapgef2*-f/f cortices, suggesting delayed migration of Rapgef2-deficient neurons in the *Cre/cEGFP* cortices (Fig. 7*A*). When the time course of migration was examined at E18.5, the proportion of GFP^+ cells in the IZ was markedly increased in the *Cre/cEGFP* cortices (Fig. 7*D*). At the same time, while 11.7 ± 3.4% of GFP^+ cells assumed multipolar morphology in the *EGFP/Rapgef2*-f/f cortices, 52.1 ± 1.3% of GFP^+ cells exhibited multipolar morphology and remained in the IZ in the *Cre/cEGFP* cortices (Fig. 7*E*), indicating the existence of a multipolar-bipolar transition defect, which was similar to that observed in mice with the Rap1GAP-mediated inactivation of

463 Rap1 or the shRNA-mediated knockdown of Rapgef2 (Jossin and Cooper, 2011; Ye *et*
464 *al.,* 2014). These results suggested that the loss of the Rapgef2 function caused transient
465 defects in the migration and multipolar-bipolar transition of post-mitotic neurons by a
466 cell-autonomous mechanism. The corresponding defects in the *Rapgef2*-cKO cortices,
467 which last to the adulthood and lead to the ECM formation, seemed to be caused by a
468 non-cell-autonomous effect.

469 The results obtained with the *EGFP/Rapgef2*-cKO cortices also revealed that almost
470 all of GFP^+ neurons failed to migrate and were localized in the IZ at P7 (Fig. 7*A, B*),
471 indicating that RGCs lining the apical surface, which could be labeled with GFP by IUE,
472 did not constitute the progenitor pool for neurons constituting the 6-layered neocortex.
473 To examine the role of ectopically-located progenitors in generating neurons in the
474 neocortex, we employed the BrdU incorporation method, which was capable of labeling
475 neural progenitors regardless of their localization. When BrdU was administered to
476 pregnant mice with *Rapgef2*-f/f and *Rapgef2*-cKO embryos at E15.5 to label late-born
477 neurons, $BrdU^+$ cells were found to be located in both the layers II-IV and the ECM at
478 P0 in the *Rapgef2*-cKO cortices while they were predominantly located in the layers
479 II-IV in the *Rapgef2*-f/f cortices (Fig. 8). These results implied that, in the E14.5

480 *Rapgef2*-cKO cerebral cortices, ectopically-located RGCs and IPCs, not RGCs located
481 in the VZ, mainly contributed to the formation of the 6-layered neocortex.
482
483 **Discussion**
484 Rap1 has been shown to play crucial roles in various processes of cortical
485 development: the preplate splitting, the multipolar-bipolar transition prerequisite for the
486 RGC-independent multipolar migration and the RGC-independent terminal
487 translocation but not the RG fiber-dependent locomotion of post-mitotic neurons (Voss
488 *et al.,* 2008; Franco *et al.*, 2011; Jossin and Cooper, 2011; Sekine *et al.,* 2012; Ye *et al.,*
489 2014). This is based on the observation of mouse embryonic brains with
490 shRNA-mediated knockdown of Rap1 or Rap1-GEFs, such as Rapgef1/C3G and
491 Rapgef2, and IUE-mediated overexpression of a dominant negative Rap1 mutant or a
492 Rap1-GAP as well as those with a hypomorphic mutation of Rapgef1/C3G. The
493 Reelin-Reelin receptors-Dab1-Crk/CrkL-Rapgef1/C3G-Rap1 pathway is involved in all
494 the Rap1-dependent processes described above although molecules downstream of
495 Rap1 seem to be different: N-cadherin for the multipolar migration and
496 multipolar-bipolar transition, and integrin $\alpha5\beta1$ and N-cadherin for the terminal
497 translocation (Voss *et al.,* 2008; Franco *et al.*, 2011; Jossin and Cooper, 2011; Sekine *et*

498 *al.,* 2012). However, it was recently reported that Rapgef2, not Rapgef1/C3G,
499 specifically governs the multipolar-bipolar transition via Rap1-N-cadherin signaling and
500 that its activity is regulated through phosphorylation by Cdk5 (Ye *et al.,* 2014). In
501 addition, Rap1 seems to be involved in other neurodevelopmental processes such as
502 dendrite development (Chen *et al.,* 2005: Srivastava *et al.,* 2012) and spine
503 morphogenesis (Xie *et al.,* 2005).

504 In this study, we demonstrated that Rapgef6 has a cooperative function with Rapgef2
505 in cortical development by showing that additional knockout of *Rapgef6* in
506 *Rapgef2*-cKO mice resulted in marked enlargement of the ECM lacking the layer
507 structure at P90 while knockout of *Rapgef6* alone did not exhibit any discernible effects
508 (Fig. 1). While the *Rapgef2*-cKO ECM was composed of late-born neurons only, the
509 *Rapgef2/6*-dKO ECM was composed of both early-born and late-born neurons,
510 suggesting earlier occurrence of developmental defects in the *Rapgef2/6*-dKO brains.
511 These observations prompted us to study the effects of *Rapgef2*-cKO and
512 *Rapgef2/6*-dKO on differentiation and migration of neural progenitors and neurons
513 during embryonic brain development. To our surprise, we found that $Pax6^+$ RGCs and
514 $Tbr2^+$ IPCs were scattered over the entire cerebral cortices and that their total numbers
515 showed a substantial increase in *Rapgef2*-cKO embryos at E15.5 and *Rapgef2/6*-dKO

516 embryos at E13.5 and E15.5 (Fig. 2). Concurrently, both mitotic cells and S phase cells,
517 which were either $Pax6^+$ or $Tbr2^+$, also showed similar cortex-wide scattering and the
518 increase in their numbers, indicating that the ectopically-located $Pax6^+$ cells and $Tbr2^+$
519 cells were proliferative and that an expansion of the progenitor pools actually occurred
520 in these mice. The IUE-mediated GFP labeling of RGCs lining the apical surface in the
521 E14.5 *Rapgef2*-cKO embryos largely confirmed the above observation; at E16.5 both
522 $Pax6^+$/GFP^+ cells and $Tbr2^+$/GFP^+ cells almost completely disappeared from the VZ and
523 were mainly located in the IZ and CP (Fig. 6*B*). Preservation of progenitor properties in
524 the ectopically-located $Pax6^+$ or $Tbr2^+$ cells was further supported by fate analysis of
525 BrdU-incorporated cells, which showed that these cells could differentiate into neurons
526 constituting the neocortex and ECM in postnatal *Rapgef2*-cKO mice (Fig. 8). These
527 results were consistent with the substantial increase in the total numbers of late-born
528 neurons in *Rapgef2*-cKO mice and both early-born and late-born neurons in
529 *Rapgef2/6*-dKO mice at P90.

530 As for the mechanism for the aberrant progenitor localization, we found that the
531 apical surfaces lining the ventricle exhibited irregular morphology and that a dense
532 array of the AJs on the apical surfaces became almost nonexistent in the *Rapgef2*-cKO
533 cortices at E15.5 and the *Rapgef2/6*-dKO cortices at E13.5 and E15.5 (Figs. 3*B*, 4). The

534 IUE-mediated GFP labeling of RGCs in the E14.5 *Rapgef2*-cKO embryos largely
535 confirmed the observations with the E15.5 *Rapgef2*-cKO cortices (Fig. 2); at E16.5 the
536 apical surface exhibited very irregular cell arrangements and not only the apical fiber
537 endfeet and their AJs but also the apical fibers themselves of $Pax6^{+}/GFP^{+}$ cells became
538 almost nonexistent (Fig. 6*D*). Thus, the extents of the structural disturbance of the
539 apical surface structure apparently correlated with those of the aberrant localization of
540 neural progenitors. The difference in the severity of the various phenotypes between
541 *Rapgef2*-cKO and *Rapgef2/6*-dKO mice seemed to be accounted for by the temporal
542 difference in the expression of Rapgef2 and Rapgef6; both Rapgef2 and Rapgef6 at
543 E13.5, but Rapgef2 only at E15.5, were expressed and concentrated on the apical
544 surface (Fig. 3). Thus, Rapgef6 was capable of compensating for the loss of Rapgef2
545 function at E13.5 but not at 15.5, which could account for the differential involvements
546 of early-born and late-born neurons in the ECM formation between *Rapgef2*-cKO and
547 *Rapgef2/6*-dKO mice (Fig. 1).

548 Analysis of the cell-autonomous effect of *Rapgef2* deletion through IUE-mediated
549 co-transduction of Cre recombinase and EGFP into the E14.5 brains revealed that at
550 E16.5 the proportion of $Pax6^{+}/GFP^{+}$ cells showed a marked decrease in the VZ, which
551 was accompanied by an increase in the proportion of GFP^{+} cells, though totally negative

552 for Pax6 or Tbr2, located in the IZ, suggesting earlier detachment of RGCs from the
553 apical surface (Fig. 6*B, C*). Moreover, the numbers of GFP^+ apical fibers and their
554 endfeet on the apical surface were substantially reduced and the apical surface AJs were
555 compromised at E16.5, which was similar to the observation with the *Rapgef2*-cKO
556 cortices (Fig. 6*D*). Intriguingly, these aberrant phenotypes were effectively suppressed
557 by the coexpression of the constitutively active Rap1 mutant, $Rap1^{G12V}$ (Fig. 6*E-G*).
558 These results indicated that Rapgef2 possesses a cell-autonomous function, governed by
559 its Rap1-GEF activity, in maintaining the apical surface AJ structures and preventing
560 earlier detachment of RGCs from the apical surface. However, a non-cell-autonomous
561 effect of the *Rapgef2* knockout seems to be responsible for the preservation of the
562 progenitor properties in RGCs and IPCs detached from the apical surface as observed in
563 the *Rapgef2*-cKO cortices. Recent studies showed that loss of the attachment of RGCs
564 to the apical surface, such as that induced by shRNA-mediated knockdown of
565 N-cadherin, led to reduction of β-catenin signaling, premature neuronal differentiation,
566 cell cycle exit and increased migration toward the CP, suggesting that earlier
567 detachment of RGCs from the apical surface might lead to premature neuronal
568 differentiation (Zhang *et al*., 2010, 2013). Presently, we have no idea of accounting for
569 the preservation of the neural progenitor properties in RGCs and IPCs of *Rapgef2*-cKO

570 embryos, which are detached from the apical surface and ectopically located. In this
571 sense, it may be noteworthy to point out that the phenotype of ectopic localization of
572 RGCs while retaining the progenitor properties was also observed in mice with
573 knockout of the AJ proteins such as N-cadherin, E-cadherin and afadin (Machon *et al*.,
574 2003; Lien *et al*., 2006; Kadowaki *et al*., 2007; Gil-Sanz *et al*., 2014; Yamamoto *et al*.,
575 2015).

576 We also observed a defect in the multipolar-bipolar transition of neurons in
577 *Rapgef2*-cKO embryos by IUE-mediated GFP-labeling of RGCs at E14.5, confirming
578 the previous report (Ye *et al.,* 2014). Almost all of GFP^+ cells, which were also $Cux1^+$,
579 failed to reach the layers II-IV and were located in the ECM of the *Rapgef2*-cKO cortex
580 at P7 and about a half of them assumed multipolar morphology (Fig. 7). The ectopic
581 accumulation of neurons observed at E15.5 was likely to be a predecessor of the ECM
582 formed in the adult *Rapgef2*-cKO and *Rapgef2*/*6*-dKO cortices. However, analysis of
583 the cell-autonomous effect of *Rapgef2* deletion through IUE-mediated co-transduction
584 of Cre recombinase and EGFP into the E14.5 brains revealed that almost all of
585 $Cux1^+/GFP^+$ neurons successfully reached the layers II-IV at P7. The $Cux1^+/GFP^+$
586 neurons exhibited multipolar morphology in a high proportion and a significant delay in
587 migration at E18.5, indicating the existence of a multipolar-bipolar transition defect.

588 These results suggested that the loss of the Rapgef2 function caused transient defects in
589 the migration and multipolar-bipolar transition of neurons in a cell-autonomous manner.
590 On the other hand, further contribution of a non-cell-autonomous effect, presumably
591 implemented by Rapgef2-deficient surroundings of the migrating neurons, was needed
592 to yield the corresponding defects in the *Rapgef2*-cKO cortices, which lasted to the
593 adulthood and led to the ECM formation. In this line, the disorganization of the RG
594 fiber system observed in the *Rapgef2*-cKO cortices may play a key role by
595 compromising neuronal migration dependent on its guidance. Indeed, a certain
596 correlation was observed between the extents of RG fiber disorganization and the
597 migration defect of Ctip2^{+} neurons (Fig. 5). However, we presently do not know how
598 neurons produced from the ectopically-located neural progenitors migrate and form the
599 apparently normal neocortex and the ECM as suggested from the BrdU-labeling
600 experiment (Fig. 8).

601 During preparation of this manuscript, analysis of brain malformations in mice
602 lacking both Rap1a and Rap1b in their cerebral cortices was reported (Shah *et al*., 2016).
603 The cerebral cortices of these mice exhibited severe developmental defects similar to
604 those observed in *Rapgef2*-cKO and *Rapgef2/6*-dKO mice in our study, which were
605 characterized by ectopic localization of neural progenitors, disruption of the AJs in the

606 VZ and impairment of the multipolar-bipolar transition. These results demonstrate the
607 crucial and predominant role of Rapgef2 and Rapgef6 in the formation of the apical
608 surface AJ structure, which is essential for the proper localization of neural progenitors,
609 and the multipolar-bipolar transition of neurons via mediating Rap1 activation
610 downstream of presently unknown extracellular stimuli. It may be noteworthy that rare
611 inherited copy number variations of the *RAPGEF6* gene, involving microdeletions of its
612 exons 2-11, were reported to exhibit strong genetic association with schizophrenia (Xu
613 *et al*., 2008). Recent study showed that *Rapgef6*-knockout mice exhibited impaired
614 function of the amygdala and hippocampus, brain regions implicated in schizophrenia
615 pathophysiology (Levy *et al.,* 2015). Moreover, a chromosomal region containing the
616 *RAPGEF2* gene was identified as a rare inherited copy number variant with a linkage to
617 schizophrenia (Xu *et al*., 2009). Further studies on Rapgef2 and Rapgef6 will help in
618 advancing our understanding of not only the fundamental mechanism for the cerebral
619 corticogenesis but also the etiology of various central nervous system diseases.
620

621 **References**

622 Bilasy SE, Satoh T, Ueda S, Wei P, Kanemura H, Aiba A, Terashima T, Kataoka T
623 (2009) Dorsal telencephalon-specific RA-GEF-1 knockout mice develop heterotopic
624 cortical mass and commissural fiber defect. Eur J Neurosci 29:1994-2008.
625 Bilasy SE, Satoh T, Terashima T, Kataoka T (2011) RA-GEF-1 (Rapgef2) is essential
626 for proper development of the midline commissures. Neurosci Res 71:200-209.
627 Boettner B, Van Aelst L (2009) Control of cell adhesion dynamics by Rap1 signaling.
628 Curr Opin Cell Biol 21:684-693.
629 Chen Y, Wang PY, Ghosh A (2005) Regulation of cortical dendrite development by
630 Rap1 signaling. Mol Cell Neurosci 28:215-28.
631 Defelipe J (2011) The evolution of the brain, the human nature of cortical circuits, and
632 intellectual creativity. Front Neuroanat 5:29.
633 de Rooij J, Boenink NM, van Triest M, Cool RH, Wittinghofer A, Bos JL (1999)
634 PDZ-GEF1, a guanine nucleotide exchange factor specific for Rap1 and Rap2. J Biol
635 Chem 274:38125-38130.
636 Englund C, Fink A, Lau C, Pham D, Daza RA, Bulfone A, Kowalczyk T, Hevner RF
637 (2005) Pax6, Tbr2, and Tbr1 are expressed sequentially by radial glia, intermediate

progenitor cells, and postmitotic neurons in developing neocortex. J Neurosci 25:247-251.

Franco SJ, Martinez-Garay I, Gil-Sanz C, Harkins-Perry SR, Müller U (2011) Reelin regulates cadherin function via Dab1/Rap1 to control neuronal migration and lamination in the neocortex. Neuron 69:482-497.

Gao X, Satoh T, Liao Y, Song C, Hu CD, Kariya K, Kataoka T (2001) Identification and characterization of RA-GEF-2, a Rap guanine nucleotide exchange factor thatserves as a downstream target of M-Ras. J Biol Chem 276:42219-42225.

Gil-Sanz C, Landeira B, Ramos C, Costa MR, Müller U (2014) Proliferative defects and formation of a double cortex in mice lacking Mltt4 and Cdh2 in the dorsal telencephalon. J Neurosci 34:10475-10487.

Gloerich M, Bos JL (2011) Regulating Rap small G-proteins in time and space. Trends Cell Biol 21:615-623.

Götz M, Huttner WB (2005) The cell biology of neurogenesis. Nat Rev Mol Cell Biol 6:777-788.

Greig LC, Woodworth MB, Galazo MJ, Padmanabhan H, Macklis JD (2013) Molecular logic of neocortical projection neuron specification, development and diversity. Nat Rev Neurosci 14:755-769.

656 Hoerder-Suabedissen A, Molnár Z (2015) Development, evolution and pathology of
657 neocortical subplate neurons. Nat Rev Neurosci 16:133-146.
658 Junghans D, Hack I, Frotscher M, Taylor V, Kemler R (2005) Beta-catenin-mediated
659 cell-adhesion is vital for embryonic forebrain development. Dev Dyn 233:528-539.
660 Jossin Y, Cooper JA (2011) Reelin, Rap1 and N-cadherin orient the migration of
661 multipolar neurons in the developing neocortex. Nat Neurosci 14:697-703.
662 Kadowaki M, Nakamura S, Machon O, Krauss S, Radice GL, Takeichi M (2007)
663 N-cadherin mediates cortical organization in the mouse brain. Dev Biol 304:22-33.
664 Kawauchi T, Chihama K, Nishimura YV, Nabeshima Y, Hoshino M (2005) MAP1B
665 phosphorylation is differentially regulated by Cdk5/p35, Cdk5/p25, and JNK.
666 Biochem Biophys Res Commun 331:50-55.
667 Levy RJ, Kvajo M, Li Y, Tsvetkov E, Dong W, Yoshikawa Y, Kataoka T, Bolshakov
668 VY, Karayiorgou M, Gogos JA (2015) Deletion of Rapgef6, a candidate
669 schizophrenia susceptibility gene, disrupts amygdala function in mice. Transl
670 Psychiatry 5:e577.
671 Liao Y, Kariya K, Hu CD, Shibatohge M, Goshima M, Okada T, Watari Y, Gao X, Jin
672 TG, Yamawaki-Kataoka Y, Kataoka T (1999) RA-GEF, a novel Rap1A guanine

673 nucleotide exchange factor containing a Ras/Rap1A-associating domain, is
674 conserved between nematode and humans. J Biol Chem 274:37815-37820.
675 Liao Y, Satoh T, Gao X, Jin TG, Hu CD, Kataoka T (2001) RA-GEF-1, a guanine
676 nucleotide exchange factor for Rap1, is activated by translocation induced by
677 association with Rap1·GTP and enhances Rap1-dependent B-Raf activation. J Biol
678 Chem 276:28478-28483.
679 Lien WH, Klezovitch O, Fernandez TE, Delrow J, Vasioukhin V (2006) alphaE-catenin
680 controls cerebral cortical size by regulating the hedgehog signaling pathway. Science
681 311:1609-1612.
682 Machon O, van den Bout CJ, Backman M, Kemler R, Krauss S (2003) Role of
683 beta-catenin in the developing cortical and hippocampal neuroepithelium.
684 Neuroscience 122:129-143.
685 Nagano T, Edamatsu H, Kobayashi K, Takenaka N, Yamamoto M, Sasaki N, Nishimura
686 Y, Kataoka T (2014) Phospholipase Cε, an effector of Ras and Rap small GTPases,
687 is required for airway inflammatory response in a mouse model of bronchial asthma.
688 PLoS One 9:e108373.
689 Nishimura YV, Shikanai M, Hoshino M, Ohshima T, Nabeshima Y, Mizutani K,
690 Nagata K, Nakajima K, Kawauchi T (2014) Cdk5 and its substrates, Dcx and

691 p27kip1, regulate cytoplasmic dilation formation and nuclear elongation in migrating
692 neurons. Development 141:3540-3550.
693 Saito T, Nakatsuji N (2001) Efficient gene transfer into the embryonic mouse brain
694 using in vivo electroporation. Dev Biol 240:237-246.
695 Schmid MT, Weinandy F, Wilsch-Bräuninger M, Huttner WB, Cappello S, Götz M
696 (2014) The role of α-E-catenin in cerebral cortex development: radial glia specific
697 effect on neuronal migration. Front Cell Neurosci 8:215.
698 Sekine K, Kawauchi T, Kubo K, Honda T, Herz J, Hattori M, Kinashi T, Nakajima K
699 (2012) Reelin controls neuronal positioning by promoting cell-matrix adhesion via
700 inside-out activation of integrin α5β1. Neuron 76:353-369.
701 Shah B, Lutter D, Tsytsyura Y, Glyvuk N, Sakakibara A, Klingauf J, Püschel AW
702 (2016) Rap1 GTPases Are Master Regulators of Neural Cell Polarity in the
703 Developing Neocortex. Cereb Cortex.
704 Shitamukai A, Konno D, Matsuzaki F (2011) Oblique radial glial divisions in the
705 developing mouse neocortex induce self-renewing progenitors outside the germinal
706 zone that resemble primate outer subventricular zone progenitors. J Neurosci
707 31:3683-3695.

708 Srivastava DP, Jones KA, Woolfrey KM, Burgdorf J, Russell TA, Kalmbach A, Lee H,
709 Yang C, Bradberry MM, Wokosin D, Moskal JR, Casanova MF, Waters J, Penzes P
710 (2012) Social, communication, and cortical structural impairments in Epac2-deficient
711 mice. J Neurosci 32:11864-11878.
712 Tsumura H, Yoshida T, Saito H, Imanaka-Yoshida K, Suzuki N (2006) Cooperation of
713 oncogenic K-ras and p53 deficiency in pleomorphic rhabdomyosarcoma
714 development in adult mice. Oncogene 25:7673-7679.
715 Voss AK, Britto JM, Dixon MP, Sheikh BN, Collin C, Tan SS, Thomas T (2008) C3G
716 regulates cortical neuron migration, preplate splitting and radial glial cell attachment.
717 Development 135:2139-2149.
718 Wei P, Satoh T, Edamatsu H, Aiba A, Setsu T, Terashima T, Kitazawa S, Nakao K,
719 Yoshikawa Y, Tamada M, Kataoka T (2007) Defective vascular morphogenesis and
720 mid-gestation embryonic death in mice lacking RA-GEF-1. Biochem Biophys Res
721 Commun. 363:106-112.
722 Xie Z, Huganir RL, Penzes P (2005) Activity-dependent dendritic spine structural
723 plasticity is regulated by small GTPase Rap1 and its target AF-6. Neuron 48:605-18.

724 Xu B, Roos JL, Levy S, van Rensburg EJ, Gogos JA, Karayiorgou M (2008) Strong
725 association of de novo copy number mutations with sporadic schizophrenia. Nat
726 Genet 40:880-885.
727 Xu B, Woodroffe A, Rodriguez-Murillo L, Roos JL, van Rensburg EJ, Abecasis GR,
728 Gogos JA, Karayiorgou M (2009) Elucidating the genetic architecture of familial
729 schizophrenia using rare copy number variant and linkage scans. Proc Natl Acad Sci
730 U S A 106:16746-16751.
731 Yamamoto H, Mandai K, Konno D, Maruo T, Matsuzaki F, Takai Y (2015) Impairment
732 of radial glial scaffold-dependent neuronal migration and formation of double cortex
733 by genetic ablation of afadin. Brain Res S0006-8993(15)00397-2.
734 Ye T, Ip JP, Fu AK, Ip NY (2014) Cdk5-mediated phosphorylation of RapGEF2
735 controls neuronal migration in the developing cerebral cortex. Nat Commun 5:4826.
736 Yoshikawa Y, Satoh T, Tamura T, Wei P, Bilasy SE, Edamatsu H, Aiba A, Kataoka T
737 (2007) The M-Ras-RA-GEF-2-Rap1 pathway mediates tumor necrosis factor-alpha
738 dependent regulation of integrin activation in splenocytes. Mol Biol Cell
739 18:2949-2959.
740 Zhang J, Woodhead GJ, Swaminathan SK, Noles SR, McQuinn ER, Pisarek AJ, Stocker
741 AM, Mutch CA, Funatsu N, Chenn A (2010) Cortical neural precursors inhibit their

742 own differentiation via N-cadherin maintenance of beta-catenin signaling. Dev Cell
743 18:472-479.
744 Zhang J, Shemezis JR, McQuinn ER, Wang J, Sverdlov M, Chenn A (2013) AKT
745 activation by N-cadherin regulates beta-catenin signaling and neuronal
746 differentiation during cortical development. Neural Dev 8:7.
747

Legends to Figures

Figure 1. Effects of the genotypes of Rapgef2 and Rapgef6 on the cortical structure at P90. ***A***, H&E-staining of the coronal sections of the brains of *Rapgef2*-f/f (*2-f/f*), *Rapgef2*-cKO (*2-cKO*), *Rapgef6*-KO (*6-KO*) and *Rapgef2/6*-dKO (*2/6-dKO*) mice. Representative specimens derived from 6 mice of each group are shown. The neocortex with the 6-layered structure (NCx), hippocampus (Hp), corpus callosum (cc) and ECM are indicated. Scale bars: 2 mm. ***B***, Immunohistological staining of the neocortex and ECM. Sections prepared as in ***A*** were immunostained for Ctip2 (*red*) and Cux1 (*green*). Representative specimens derived from 6 mice of each group are shown. WM, white matter. Scale bars: 100 μm. ***C***, ***D***, Distributions of $Ctip2^+$ and $Cux1^+$ neurons in the neocortex and ECM. Sections stained as in ***B*** were employed for quantification of $Ctip2^+$ neurons (*red*) and $Cux1^+$ neurons (*green*), residing in each bin, as described in Materials and Methods (***C***). The neurons contained in a total of 10 bins (100 μm in width) were counted as described in Materials and Methods (***D***). Data are expressed as the means ± SDs derived from 6 mice of each genotype. Student's t test: *$p < 0.05$, **$p < 0.01$.

Figure 2. Effects of the genotypes of Rapgef2 and Rapgef6 on distribution of neural progenitor cells. ***A***, Immunohistological detection of $Pax6^+$ cells, $Tbr2^+$ cells as and

766 BrdU-labeled S phase cells. Colonal sections of the brains of *Rapgef2*-f/f (*2-f/f*),
767 *Rapgef2*-cKO (*2-cKO*), *Rapgef6*-KO (*6-KO*) and *Rapgef2/6*-dKO (*2/6-dKO*) embryos at
768 E13.5 and E15.5, which had been subjected to BrdU labeling, were subjected to
769 immunostaining for Pax6 (*green*), Tbr2 (*cyan*) and BrdU (*red*). Pial and apical surfaces
770 of the cortices are indicated by white lines. The images are representative of 4
771 biological replicates of each group. Scale bars: 100 μm. ***B***, ***C***, Distribution of $Pax6^+$
772 cells and $Tbr2^+$ cells in the cerebral cortices. Brain sections prepared and stained as in ***A***
773 were subjected to quantification of $Pax6^+$ cells (*green lines*) and $Tbr2^+$ cells (*red lines*),
774 residing in each bin, as described in Materials and Methods (***B***). Data are expressed as
775 the means ± SDs derived from at least 4 biological replicates. The progenitors contained
776 in a total of 10 bins (100 μm in width) were counted as described in Materials and
777 Methods (***C***). Data are expressed as the means ± SDs derived from 4 mice of each
778 genotype. Student's t test: *$p < 0.05$, **$p < 0.01$. ***D***, Immunohistological detection of
779 $Pax6^+$ cells, $Tbr2^+$ cells and $pHH3^+$ metaphase cells. Brain sections prepared as in ***A***
780 were subjected to immunostaining for Pax6 (*green*), Tbr2 (*cyan*) and pHH3 (*red*). Pial
781 surfaces are indicated by white lines. The images are representative of 4 biological
782 replicates of each group. Scale bars: 100 μm. ***E***, ***F***, Ectopic localizaion of $Pax6^+$ and
783 $Tbr2^+$ metaphase cells. The percentages of the ectopically localized somata of

pHH3$^+$/Pax6$^+$ cells in the total pHH3$^+$/Pax6$^+$ cells contained in the 10 bins (100 μm in width) were determined using the immunostained sections described in ***D*** (***E***). Also, pHH3$^+$/Pax6$^+$ cells and pHH3$^+$/Tbr2$^+$ cells in a total of 10 bins (100 μm in width) were counted. Data are expressed as the means ± SDs derived from 4 mice of each genotype. Student's t test: **$p < 0.01$.

Figure 3. Expression of Rapgef2 and Rapgef6 in the E13.5 and E15.5 brains. ***A***, Immunohistological detection of Rapgef2 and Rapgef6. Coronal sections of the brains of *Rapgef2*-f/f (*2-f/f*), *Rapgef2*-cKO (*2-cKO*) and *Rapgef6*-KO (*6-KO*) embryos at E13.5 and E15.5 were subjected to immunostaining for Rapgef2 or Rapgef6 (*red*) and 4',6-diamidino-2-phenylindole (DAPI) (*blue*). Scale bars: 100 μm. ***B***, Preferential expression of Rapgef2 and Rapgef6 on the apical surfaces. Coronal sections of the brains of the E13.5 and E15.5 embryos with the indicated genotypes were subjected to immunostaining for Rapgef2 or Rapgef6 (*green*), β-catenin (*red*) and DAPI (*blue*). The images are representative of 4 biological replicates of each group. Scale bars: 20 μm.

Figure 4. Effects of the genotypes of Rapgef2 and Rapgef6 on the apical surface structures. ***A***, ***B***, Immunohistological detection of proteins constituting the AJs. Coronal sections of the brains of *Rapgef2*-f/f (*2-f/f*), *Rapgef2*-cKO (*2-cKO*), *Rapgef6*-KO (*6-KO*) and *Rapgef2/6*-dKO (*2/6-dKO*) embryos at E13.5 (***A***) and E15.5 (***B***) were subjected to

802 immunostaining for β-catenin (*β-cat.*), N-cadherin (*N-cad.*), E-cadherin (*E-cad.*), afadin
803 and ZO-1 as indicated. The leftmost panels are phase contrast images with a lower
804 magnification. The images are representative of 4 biological replicates of each group.
805 Scale bars: 100 μm (*leftmost panels*) and 10 μm (*other panels*).

806 **Figure 5.** Effects the genotypes of Rapgef2 and Rapgef6 on RG fiber organization and
807 neuronal migration. ***A***, Morphology of RG fibers. Coronal sections of the brains of
808 *Rapgef2*-f/f (*2-f/f*), *Rapgef2*-cKO (*2-cKO*), *Rapgef6*-KO (*6-KO*) and *Rapgef2/6*-dKO
809 (*2/6-dKO*) embryos at E13.5 and E15.5 were subjected to immunostaining for nestin.
810 The images are representative of 3 biological replicates of each group. Scale bars: 50
811 μm. ***B***, Morphology of ectopically-located GFP-labeled cells. RGCs lining the apical
812 surface of the *Rapgef2*-f/f (*2-f/f*) and *Rapgef2*-cKO (*2-cKO*) cortices were labeled with
813 GFP by IUE of pCAG-EGFP-F at E14.5 and the morphology of their progenies was
814 analyzed at E15.5 by immunohistological staining for GFP (*green*) and Pax6 (*red*).
815 $GFP^+/Pax6^+$ RGCs are indicated by arrowheads. The apical and pial surfaces of the
816 telencephalon were indicated by white broken lines. The images are representative of 4
817 biological replicates of each group. Scale bars: 20 μm ***C***, Localization of $Ctip2^+$ neurons.
818 Colonal sections of the brains of the E13.5 and E15.5 embryos with the indicated

genotypes were subjected to immunostaining for Ctip2 (*red*) and DAPI (*blue*). The images are representative of 3 biological replicates of each group. Scale bars: 50 μm.

Figure 6. Phenotypes of Cre-mediated *Rapgef2* knockout and compensatory effects of artificial Rap1 expression. ***A***, Efficient knockout of *Rapgef2* by introduction of Cre recombinase. *Rapgef2*-f/f (*2-f/f*) embryos at E14.5 were subjected to IUE-mediated transduction of pCAG-NLS-Cre and pCAG-FloxP-EGFP-N1 (*Cre/cEGFP*). As controls, *Rapgef2*-cKO (*2-cKO*) and *Rapgef2*-f/f embryos at E14.5 were subjected to IUE-mediated transduction of CAG=EGFP (*EGFP*). Colonal sections of the brains of *Cre/cEGFP* and *EGFP/Rapgef2*-f/f embryos at E16.5 were subjected to immunostaining for GFP (*green*) and Rapgef2 (*red*) as indicated. GFP^+ cells apparently lacking Rapgef2 expression are indicated by arrowheads. The images are representative of 4 biological replicates of each group. Scale bars: 20 μm. ***B***, ***C***, Zonal distribution of GFP-labeled cells and their neural progenitor markers. The sections prepared as in ***A*** were subjected to immunostaining for GFP (*green*), Pax6 (*red*) and Tbr2 (*purple*) (***B***). The images are representative of 4 biological replicates of each group. Scale bars: 50 μm. The percentages of GFP^+ cells located in the VZ, SVZ and IZ/CP (*left*) and those displaying $Pax6^-/Tbr2^-$ (*D.N.*), $Pax6^+$ and $Tbr2^+$ markers (*right*) are shown as the means ± SDs derived from 4 each of *EGFP/Rapgef2*-ff (*white bars*) and *Cre/cEGFP* (*purple*

837 *bars*) embryos (***C***). Student's *t* test: **p* < 0.05, ***p* < 0.01. ***D***, Disruption of the apical
838 surface structures by Cre-mediated *Rapgef2* knockout. The sections prepared as in ***A***
839 were subjected to immunostaining for GFP (*green*), afadin (*red*) and Pax6 (*blue*) as
840 indicated. The images are representative of 4 biological replicates of each group.
841 Arrowheads indicate the endfeet of the apical fibers of GFP-labeled RGCs on the apical
842 surface. Scale bars: 50 μm. ***E***, ***F***, Effects of the overexpression of constitutively active
843 Rap1 on zonal distribution of GFP-labeled cells and their neural progenitor markers.
844 Either pCAG-Myc-Rap1^{WT} (*Rap1^{WT}*), pCAG-Myc-Rap1^{G12V} (*Rap1^{G12V}*) or pCAG-Myc
845 (*Vector*) were co-transduced by IUE with pCAG-NLS-Cre and pCAG-FloxP-EGFP-N1
846 into *Rapgef2*-f/f (*2-f/f*) embryos at E14.5. Colonal sections of the brains at E16.5 were
847 subjected to immunostaining for GFP (*green*), Pax6 (*red*) and Tbr2 (*purple*) as indicated
848 (***E***). The images are representative of 3 biological replicates of each group. Scale bars:
849 50 μm. The percentages of GFP$^+$ cells located in the VZ, SVZ and IZ/CP (*left*) and
850 those displaying Pax6$^-$/Tbr2$^-$ (*D.N.*), Pax6$^+$ and Tbr2$^+$ markers (*right*) are shown as the
851 means ± SDs derived from 3 each of mice co-transduced with either pCAG-Myc
852 (*purple bars*), pCAG-Myc-Rap1^{WT} (*yellow bars*) and pCAG-Myc-Rap1^{G12V} (*red bars*)
853 (***F***). Student's *t* test: ***p* < 0.01. ***G***, Effects of Rap1 overexpression on the apical surface
854 structures of Cre-mediated *Rapgef2* knockout. The sections prepared as in ***E*** were

855 subjected to immunostaining for GFP (*green*), ZO-1 (*red*) and Myc (*blue*) as indicated.
856 The images are representative of 3 biological replicates of each group. Arrowheads
857 indicate the endfeet of the apical fibers of GFP-labeled cells on the apical surface. Scale
858 bars: 50 μm.

859 **Figure 7.** Effects of *Rapgef2* knockout on the morphology and migration of neurons. ***A***,
860 ***B***, Effects of *Rapgef2* knockout on neuronal migration observed at P7. *Rapgef2*-f/f
861 (*2-f/f*) embryos at E14.5 were subjected to IUE-mediated transduction of
862 pCAG-NLS-Cre and pCAG-FloxP-EGFP-N1 (*Cre/cEGFP*). As controls, *Rapgef2*-cKO
863 (*2-cKO*) and *Rapgef2*-f/f embryos at E14.5 were subjected to IUE-mediated
864 transduction of CAG=EGFP (*EGFP*). Colonal sections of the brains at P7 were
865 subjected to immunostaining for GFP (*green*), Cux1 (*red*), Ctip2 (*red*) and DAPI (*blue*)
866 as indicated (***A***). Due to the nuclear localizing nature of EGFP, double staining with
867 Cux1 or Ctip2 is recognizable only in the nuclei. Images shown are representative of 4
868 biological replicates of each group. The layers II-IV and V-VI and the ECM are
869 indicated. The apical surfaces of the cortices are indicated by white lines. Scale bars:
870 100 μm. The percentages of GFP^+ cells located in the layers II-IV, V-VI and the ECM
871 (*left*) and those displaying $Cux1^+$, $Ctip2^+$ and $Cux1^-/Ctip2^-$ (*D.N.*) markers (*right*) are
872 shown as the means ± SDs derived from 8 *EGFP/Rapgef2*-f/f embryos (*white bars*), 4

873 *EGFP/Rapgef2*-cKO embryos (*blue bars*) and 4 *Cre/EGFP* embryos (*purple bars*) (***B***).
874 ***C***, Morphology of $GFP^+/Cux1^+$ neurons located in the ECM of the *Rapgef2*-cKO
875 embryo at P7. A brain section of the *EGFP/Rapgef2*-cKO embryo prepared as in ***A*** was
876 subjected to immunostaining for GFP (*green*) and Cux1 (*red*). The right panel shows a
877 magnified image of the area surrounded by a broke line. Scale bars: 50 μm. ***D***, Effects
878 of Cre-mediated *Rapgef2* knockdown on neuronal migration observed at E18.5. Colonal
879 sections of the brains were prepared at E18.5 from the *Cre/EGFP* and
880 *EGFP/Rapgef2*-f/f embryos generated by IUE at E14.5 as described in ***A*** and subjected
881 to immunostaining for GFP (*green*) and DAPI (*blue*). The images are representative of
882 4 biological replicates of each group. The apical surfaces of the cortices are indicated by
883 white lines. Scale bars: 100 μm. ***E***, Morphology of GFP^+ cells located in the IZ at E18.5.
884 The brain sections of the E18.5 *Cre/EGFP* and *EGFP/Rapgef2*-f/f embryos IUE were
885 subjected to immunostaining for GFP (*green*), Pax6 (*red*) and Tbr2 (*blue*). Left panels
886 (**a**-**c**) are magnified images of the corresponding areas surrounded by broken lines.
887 Scale bars: 50 μm.

888 **Figure 8.** Distribution of neurons derived from neural progenitors labeled by BrdU at
889 E15.5. Neural progenitors in E15.5 *Rapgef2*-f/f (*2-f/f*) and *Rapgef2*-cKO (*2-cKO*)
890 embryos were labeled by BrdU and neurons derived from them were detected by

immunohistological staining for BrdU at P0. Nuclei were stained with DAPI. The layers II-IV, V-VI and the ECM are indicated. Images shown are representative of 4 biological replicates of each group. Scale bars: 100 µm.

Fig. 1

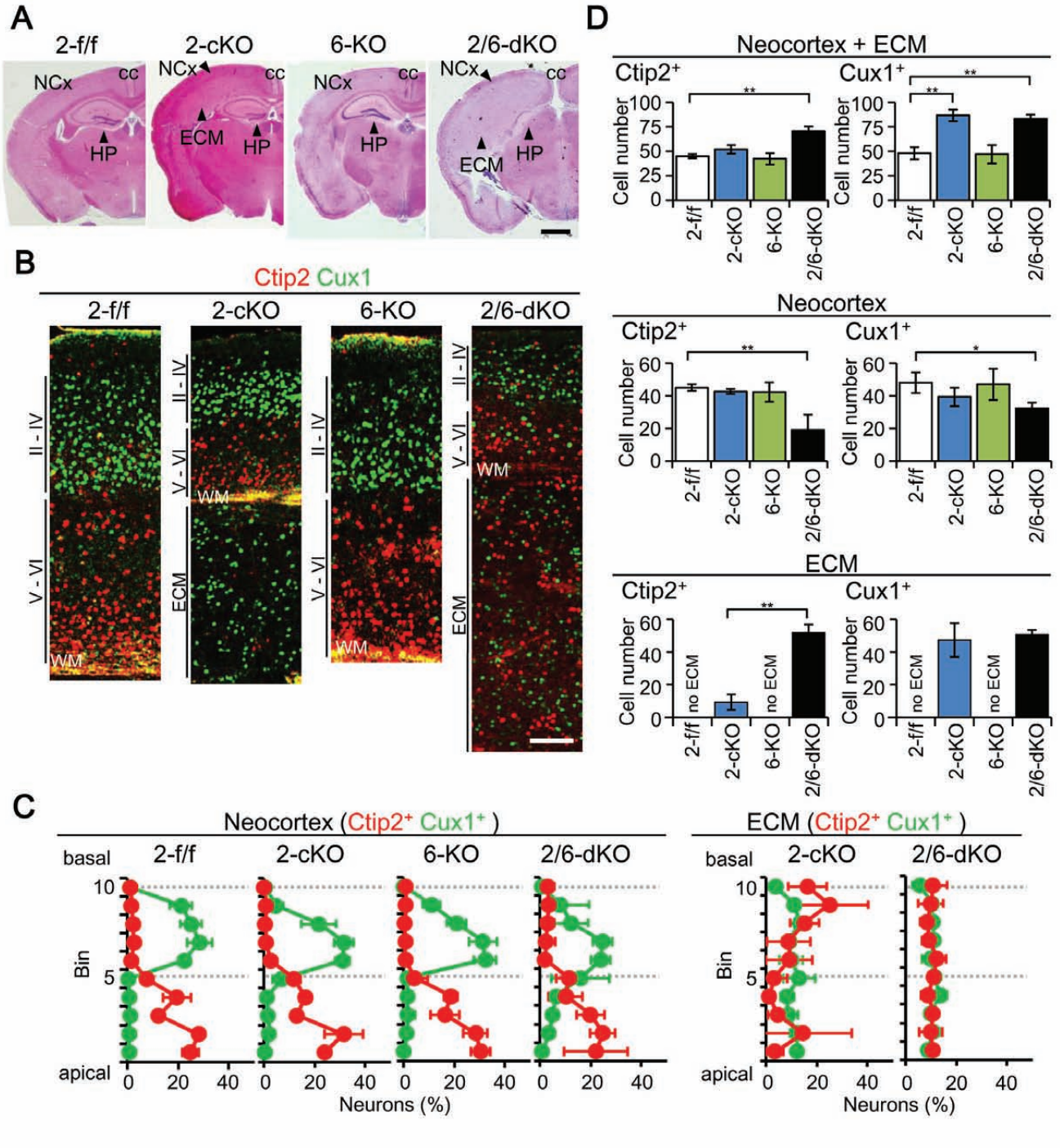

Fig.2

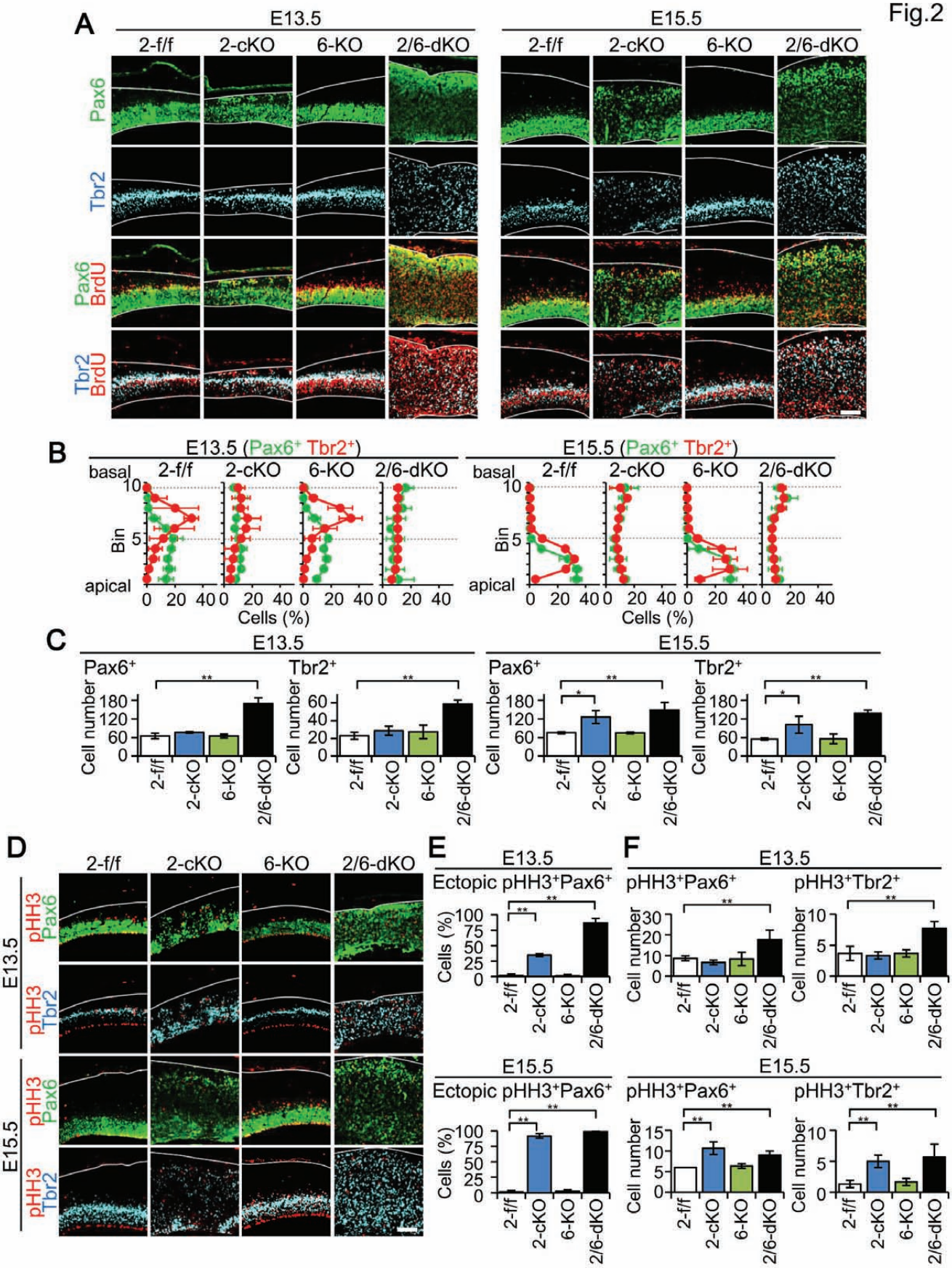

Fig.3

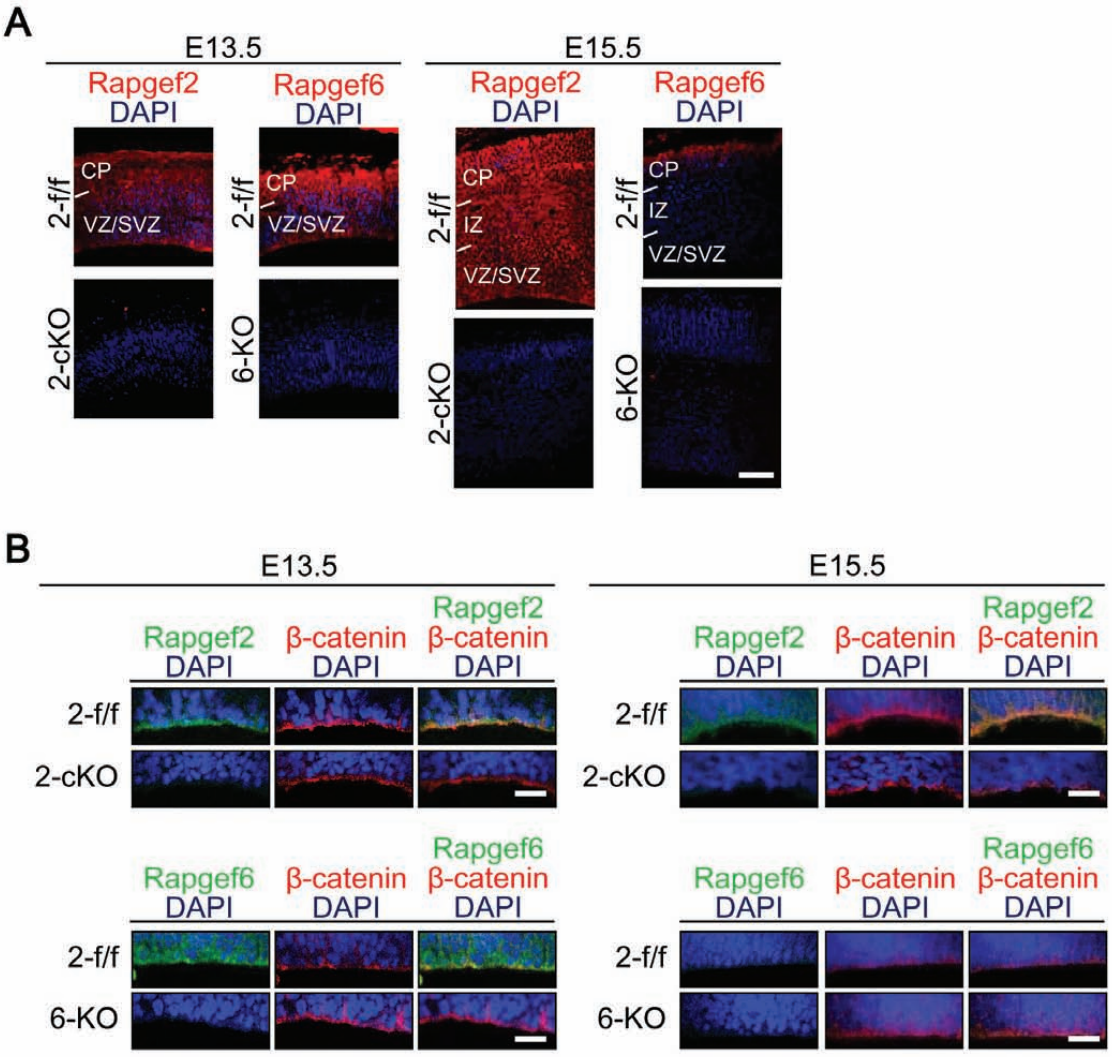

Fig.4

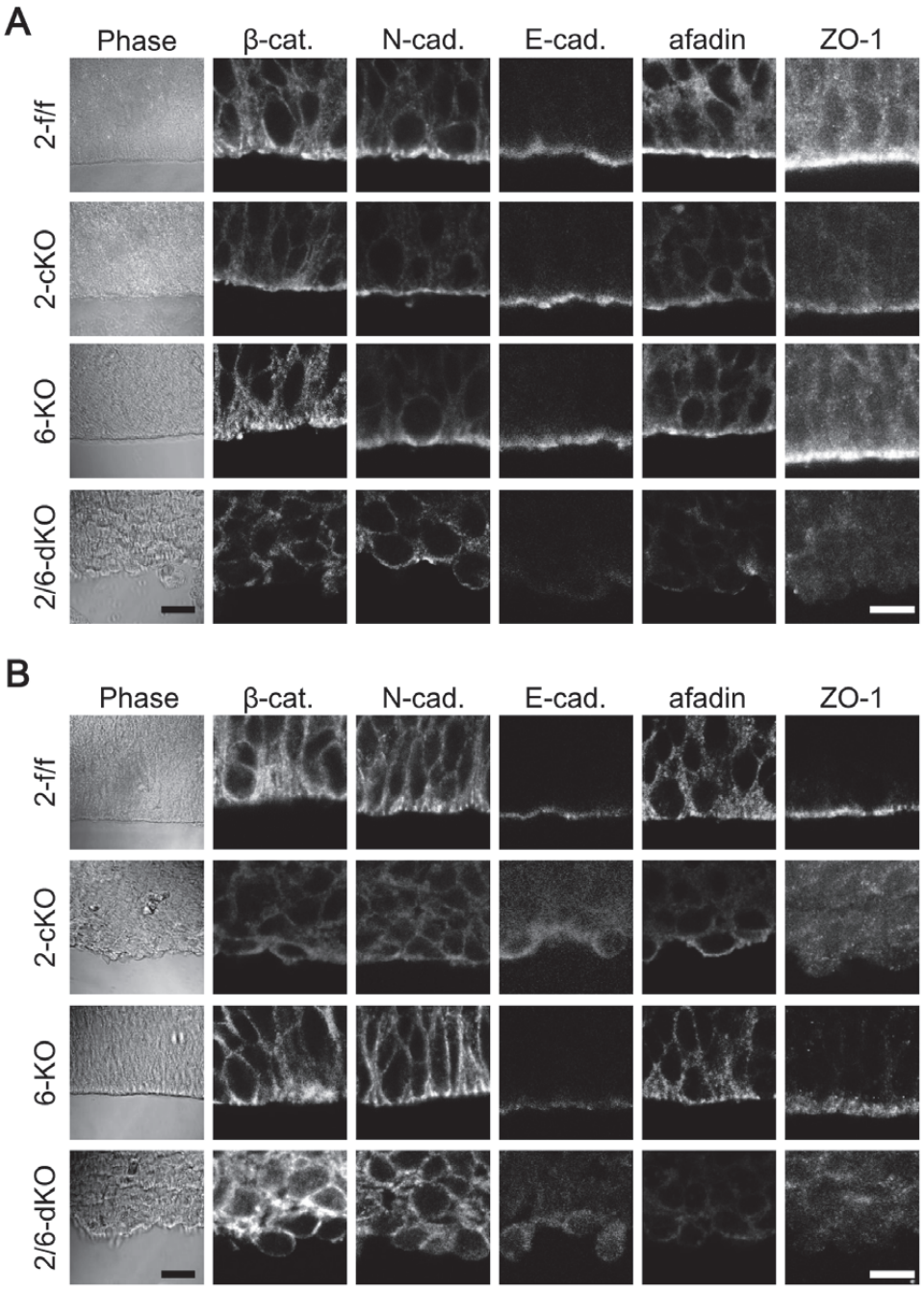

Fig.5

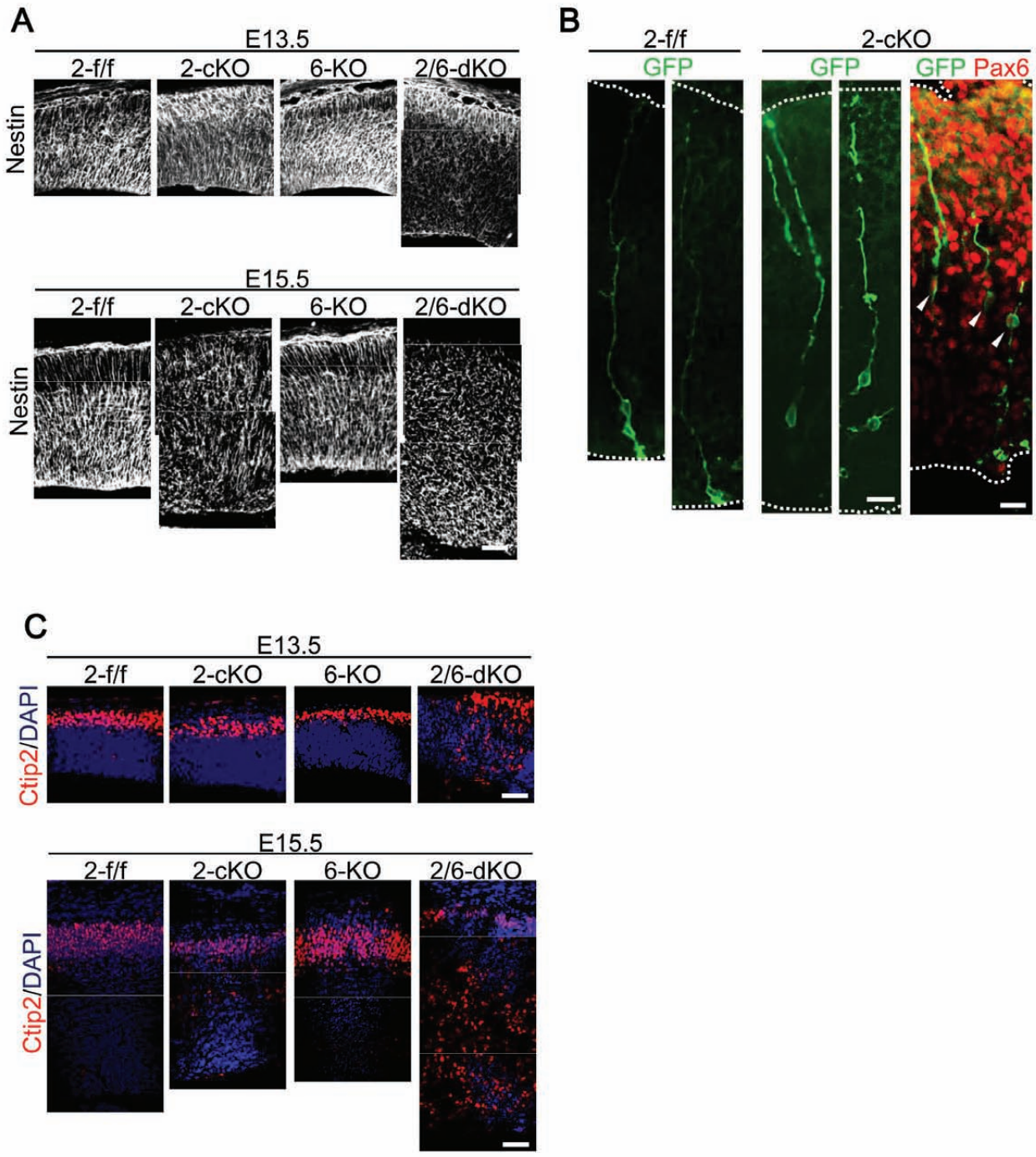

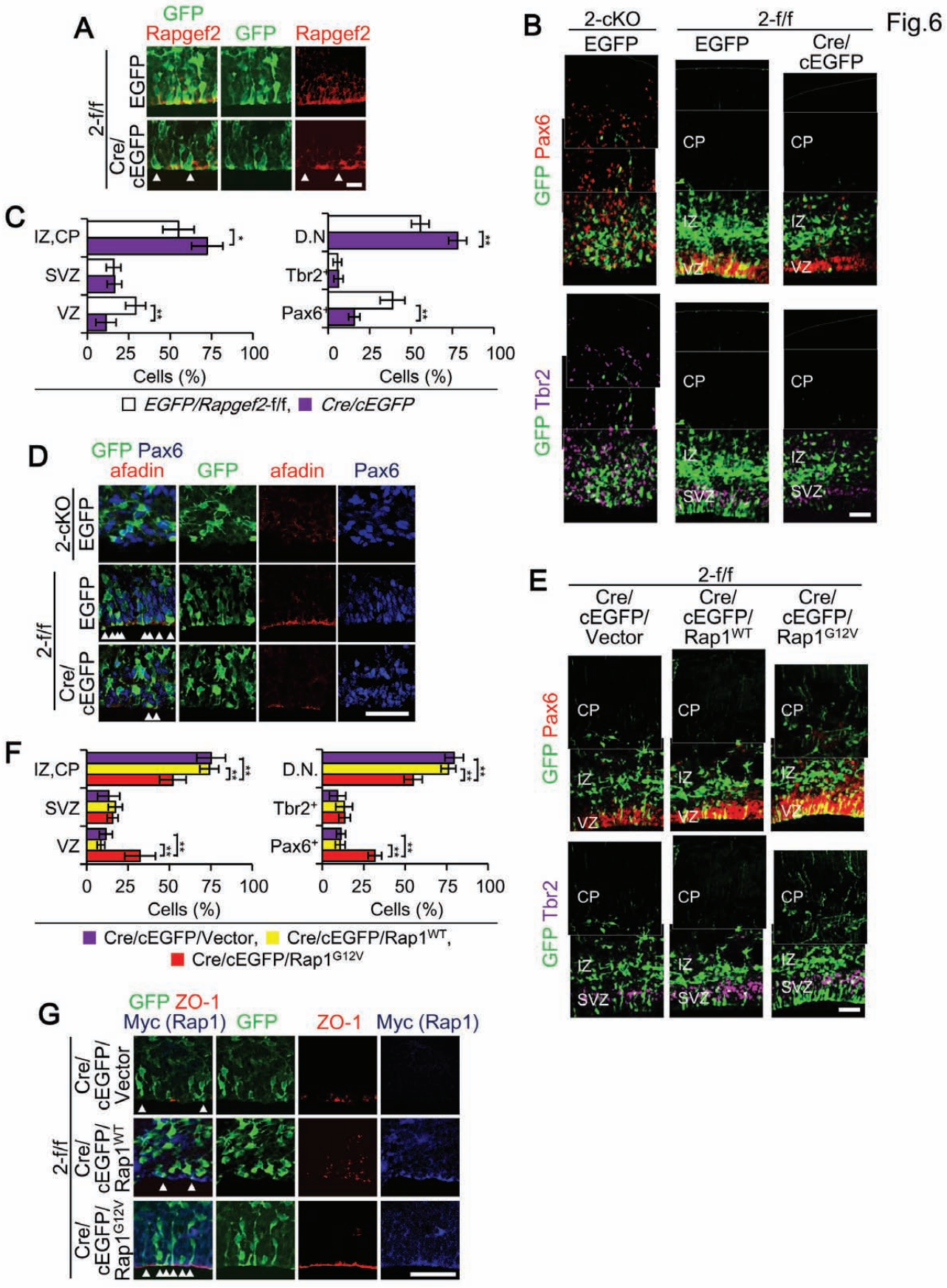

Fig.6

Fig.7

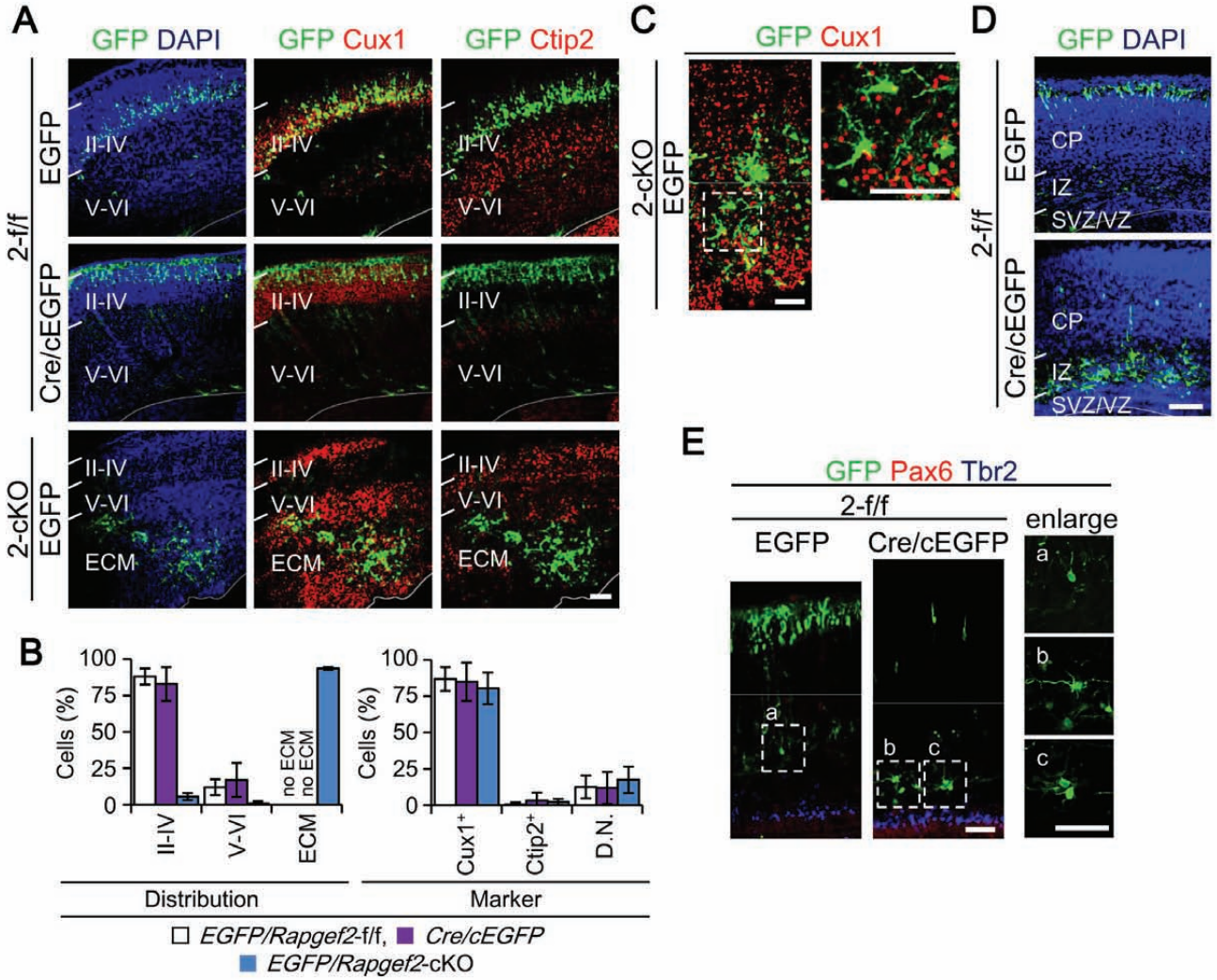

Fig.8